ELSEVIER

Contents lists available at ScienceDirect

International Journal of Fatigue

journal homepage: www.elsevier.com/locate/ijfatigue



Fatigue driving force of riveted shear joints in bridges — Replacing the net section stress

Johan Maljaars a,b,*, Sjoerd Hengeveld a,b, Jorrit Rodenburg a

- a TNO, Molengraaffsingel 8, Delft, 2629 JD, The Netherlands
- ^b Eindhoven University and Technology, Groene Loper 3, Eindhoven, 5612 AE, The Netherlands

ARTICLE INFO

Keywords:
Fatigue test database
Riveted joints
Double covered joints
Stress concentration factor
Hoop stress

ABSTRACT

Many old steel bridges contain hot riveted double strap butt joints. The fatigue life of these joints is subject of growing concern. We collected 629 fatigue tests, showing that the fatigue resistance expressed as the net section stress range is extremely scattered. Based on the theory of mechanics and the finite element method, we developed analytical equations to estimate the hoop stress range in the plate at the rivet hole. Using this stress parameter, the scatter in fatigue resistance reduces significantly. The model also gives insight into how the joint geometry influences the fatigue resistance.

1. Introduction

Hot riveting was the main joining method in steel bridges before 1950 and it has been applied until late in the years 1970. In hot riveting, rivets composed of a shaft and a shop head are heated before being installed in the holes in plates or sections. The rivet field head is subsequently created by hammering the edge of the inserted shaft [1]. Contraction during cooling causes the rivets to clamp the plates. Friction between the plates transfers part of the shear load if the assembled joint is loaded in shear in service. Clamping thus has a positive influence on the fatigue resistance of riveted joints. Many bridges with riveted joints are still in service to-date, and they are facing (rail or road) traffic volumes excessively higher than anticipated in their design. With their age increasing, the fatigue resistance of the riveted joints is subject of growing concern [2–7].

The fatigue resistance of riveted joints is often expressed in terms of the net section stress range $\Delta\sigma_{net}$, i.e., the average stress in the cross-section reduced by the holes, see Fig. 1(a). Refs. [8–12] provide a single net section stress range versus fatigue life curve (S–N curve) for all riveted details. However, the actual force transfer and the stress distribution in the joint are complex, the variations in geometry of these joints are large, and the clamping force and friction coefficient are subject to significant scatter. This causes a large scatter of predicted versus tested fatigue lives. To reduce the scatter, Taras and Greiner [13] proposed different S–N curves for different joint types. In the current study, we consider double covered joints as displayed in Fig. 2. Even for this single joint type, different studies [13–17] recommend significantly different fatigue resistances based on tests.

Significant differences between tests were observed already in the years 1930. Wilson [18] showed a large influence of geometry on the fatigue resistance of double lap joints. Graf [19–21] was the first pointing to the influence of the ratios between bearing stress, rivet shear stress and net section stress. In the years 1950, Baron and Larson [22–24] conducted a systematic study into the influence of various geometric parameters on the fatigue resistance. Parola et al. [25] extended a preliminary study of Lewitt et al. [26] into the influence of bearing, rivet clamping, and stress ratio on the fatigue resistance. However, because of the large scatter in fatigue resistance, the limited number of tests per series, and the complicated force distribution in riveted joints, these studies have not resulted in a quantified recommendation to account for bearing in the fatigue resistance of a given geometry.

More recently, the use of the Finite Element (FE) method has enabled the evaluation of the stress near the edge of the rivet hole [14, 27,28], allowing for the quantification of the geometric influence on that stress. These studies are limited to applications to one or a few geometries. Based on similar FE models, we have developed an analytical model consisting of closed-form equations to estimate the maximum tangential normal stress in the plate at the hole edge in riveted double covered joints – referred to as hoop stress σ_h , see Fig. 1(b). We applied this analytical model to a large database of double covered joints to check its performance in predicting the fatigue resistance. Our hypothesis is that the net section stress, as used to-date in the assessment of these joints in bridges, is not representative of the fatigue driving force, and it is not a good indicator of the fatigue resistance. We will show

^{*} Corresponding author at: Eindhoven University and Technology, Groene Loper 3, Eindhoven, 5612 AE, The Netherlands. E-mail address: johan.maljaars@tno.nl (J. Maljaars).

Nomenclature				
Operators				
ΔX	Range of cycle <i>X</i>			
$\mathbb{E}(X)$	Expectation of variable <i>X</i>			
$\mathbb{S}(X)$	Standard deviation of variable <i>X</i>			
$\mathbb{V}(X)$	Coefficient of variation of variable <i>X</i>			
\overline{X}	Mean of cycle X			
Symbols				
β	Bearing ratio			
μ	Friction coefficient			
ν	Poisson ratio			
σ	Stress			
σ_u	Tensile strength			
$\sigma_{cl,0}$	Rivet clamping stress before load applica-			
21,0	tion			
σ_{cl}	Rivet clamping stress			
σ_h	Hoop stress in ply at rivet hole			
σ_{net}	Net section stress			
σ_{nl}	Stress correction during unloading			
σ_p	Ply prestress caused by rivet clamping			
a	Hutchinson's factor			
a_1, a_2	Constants in the equation for $K_{t,pin}$			
b	Parameter of the lognormal distribution			
b_1, b_2	Exponents in the equation for $K_{t,pin}$			
C	Location parameter of the Basquin equation			
C'	Location parameter of the 6PRFLM			
E	Young's modulus			
e	End distance			
F	Applied force			
f	Force fraction			
f_{R}	Stress ratio correction for net stress			
f_{Rh}	Stress ratio correction for hoop stress			
G	Shear modulus			
h	Semi grip			
k	Spring stiffness			
K_t	Stress concentration factor			
$K_{t,fric}$	Stress concentration factor for frictional load			
$K_{t,hole}$	Stress concentration factor at a hole			
$K_{t,pin}$	Stress concentration factor for pin loading			
$K_{t,s}$	Stress concentration factor for a single rivet			
l'	Fatigue limit in the 6PRFLM			
L_1, L_2	Parameters of a lognormal distribution			
m	Inverse slope of the Basquin equation			
m'	Inverse slope parameter of the 6PRFLM			
N	Number of cycles			

that the hoop stress estimated with the analytical model has greater predictive capability for the fatigue resistance.

2. Description of the test data

We assume the fatigue performance of double lap joints to be equal to that of double strap butt joints. We collected 629 fatigue test results on double strap butt and double lap joints from 20 sources. All data comprise carbon steel specimens; data from puddle iron [14, 15,29,30] and manganese, silicon, or nickel steels [18,31] are not

	N. 1. C						
n_{pr}	Number of rivets per row						
n_{row}	Number of rivet rows						
n_{test}	Number of tests						
p	Pitch						
p'	Curvature parameter of the 6PRFLM						
R	Net section stress ratio						
r	Hole radius						
R_h	Hoop stress ratio						
r_o	Cone outer radius						
R_{sq}	Coefficient of determination						
t_p	Semi ply thickness						
t_s	Thickness of one strap or lap plate						
и	Deformation						
w	Semi plate width						
Subscripts (multiple used)							
μ	Accounting for friction						
C	Characteristic value						
i	Of rivet row i						
ms	Of mill scale contact						
p	Of the ply						
rlp	Of red lead paint						
r	Of the rivet						
slip	At which slip occurs						
S	Of the strap or lap plate						
z	In plate thickness direction						
Superscripts (multiple used)							
FE	According to the finite element method						
max	At maximum load of the cycle						
min	At minimum load of the cycle						
t	At tipping point, i.e. at load causing slip in						
	compression						

considered. Tests with staggered rivet patterns [24,32] are also not considered. Most data stem from specimens made for the purpose of testing. Tested joints taken from actual bridges are selected only if they are reported free from corrosion and without any theoretical fatigue damage (e.g., because their location was close to the neutral axis of a beam in bending). Table 1 provides the data, where geometric symbols refer to Fig. 3, σ_u is the ply tensile strength and n_{test} is the number of tests (summation of failed specimens and run-outs). The radius r refers to the hole; the rivet has a smaller nominal radius, but it has almost the same radius as the hole after driving [18,21]. Rivet rows are counted from outside to inside, so the first row is the furthest away from the splice.

The surface finish influences the friction coefficient. A number of specimens has Red Lead Paint (RLP) or a similar coating applied on the plate faces; all other specimens have direct contact between the mill scales. The clamping force of some of these is reduced to almost zero before conducting the tests, by machining away most of the rivet head or by pressing the rivet head to detrude the shank [25] or by using pins instead of rivets [33]. We conducted three additional tests, also given in Table 1. The database is available through the supplementary material, see Appendix A.

The summed strap thickness is always equal to or larger than the ply thickness in bridge joints. Out of the 30 tests conducted with $2t_s=2t_p$, only two failed in the lap plate, a few were run-outs, and all others failed in the ply. Therefore, this study considers ply failure only. Ply failure occurred in the first rivet row – the row furthest away from the splice (Fig. 3) – in all joints.

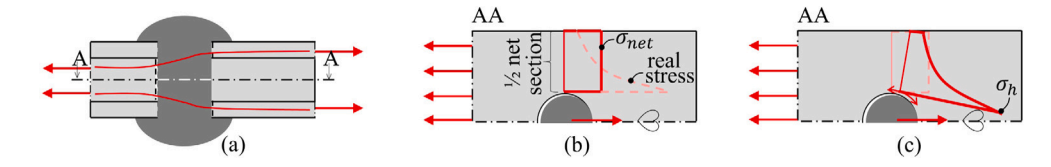


Fig. 1. Definition of stress used in fatigue assessment: (a) Side view; (b) Net section stress, σ_{net} ; (c) Hoop stress, σ_h .

Table 1
Rivet double lap and double strap joint fatigue test database

L;S ^a	n_{row}	n_{pr}	r [mm]	w [mm]	t _p [mm]	t _s [mm]	p; e ^b [mm]	RLP ^c	σ_u [MPa]	n _{test}	R	Source
S	2	1	8.5	35	6	8	70	No	410–590	74	0.09-0.38	[31]
s S	2	1	8.5	35 35	6	8	70 70	Yes	590	10	0.09-0.38	[31]
S	2	1	8.5	35	6	8	70	Yes	590	4 ^d	0.13-0.15	[20]
S	2	1	10	40-61	5–13	9–13	70	No	537–572	37	0.03-0.13	[20]
S	2	2	10	48	6.5	10	70	No	561	6	-1-0.03	[20]
S	3	2	10	66	6.5	10	70	No	567	4	-1-0.03	[20]
S	1	1	10	35	6–8	10	50	No	386	24	0-0.67	[19]
S	2	2	10	39–59	5–8.5	6.5–13	70	No	514–562	25	-1-0.03	[21]
S	2	1	11.5	58	7.5	10	80	Yes ^e	f	31	0	[34]
S	3	1	10	40	6	10	100	Yes	365	3	0	[34]
L	1	2	14.3	76	9.5	9.5–13	45–64	No	423–431	12	0	[18]g
L	2	1	14.3	52–74	4.7–9.5	9.5–13	102	No	434–442	9	0	[18]
L	2	2	14.3	45–52	6.4–9.5	9.5-52	102–152	No	439–447	13	-1-0.5	[18]
L	3	1		43–32 64–74	6.4–9.5	9.5–31	102–132			6	0	[18]
L L	3	2	14.3 14.3	43–46	9.5	9.5-29 9.5	76	No	426–437 439	4		
								No		9	-1-0	[18]
L	4	1 3	14.3	64–89	6.4–13	9.5–25	76–102	No	429–438		0	[18]
S	1		10	38	6.4–13	9.5–16	76 20	No	446	6	0	[35]
S	2	1	6.5	35	5	6	39	No	f	3	0.2	[36]
S	2	1	8.5	50	6	8	51	No	f	3	0.2	[36]
S	2	2	8.5	25	7	10	48	No	f	5	0.1	[37]
S	4	1	8.5	50	7	10	48	No		4	0.1	[37]
L	2	1	10.3	40	7.1	9.5	89	No	484	5	0	[38]
L	2	2	10.3	40	7.1	9.5	89	No	397–419	17	0	[38]
L	2	2	10.3	45	7.1	10–44	76	No	434–443	6	0	[23]
S	2	3	10.3	41	7.1	8–32	76	No	454	37	0	[22]
L	2	2	11.9	45	8.7	14	89	No	438	6	0	[24]
L	2	2	13.5	50	10	13–38	89	No	434	12	0	[24]
L	2	3	10.3	40	7.1	16	89	No	411–442	12	0	[24]
L	2	3	11.9	43	8.7	14	89	No	438	6	0	[24]
L	2	3	13.5	47–54	10	13	89	No	434	11	0	[24]
L	3	2	10.3	55	7.1	16	89	No	442	12	0	[24]
L	3	2	13.5	69	10	13–38	89	No	434	12	0	[24]
L	3	3	10.3	51–61	7.1	16	89	No	442	12	0	[24]
L	3	4	10.3	48	8.7	13	57–152	No	447–476	18	0	[24]
L	4	3	10.3	62	7.1	16	89	No	411	6	0	[24]
L	3	3	10.3	36	9.5	9.5	76	No	432	6	-1	[39]
S	2	2	10	50	6	13	100	Yes	365	3	0.25	[40]
L	2	2	11.9	43-73	4.8-9.6	6.4–12	85-146	No	438-475	81	-1-0.5	[25]
L^h	2	2	11.9	43-73	4.8-9.6	6.4–12	85–146	No	438-475	36	-1-0.5	[25]
S	2	2	7.5	25	5	6	45	Yes	f	10	0	[41]
S	2	1	10	30	7.5	10	60	Yes	f	12	0	[41]
S	2	1	9.5	25	4	8	56	No	f	10	0.01	[32]
S^h	1	1	11.5	30	4	8	35	No	f	6	0.1	[33]
S	1	1	13	40	10	10	81	Yes	518	1	0	i
S	1	1	13	40	10	10	81	No	518	2	0	i

 $^{^{}a}\ L=$ double lap joint; S= double strap butt joint.

Fig. 4(a) provides the number of cycles to failure or to the end of test, N, as a function of the net section stress range, $\Delta \sigma_{net}$, of all tests:

$$\Delta\sigma_{net} = \frac{\Delta F}{n_{pr} 2t_p (2w - 2r)} \tag{1}$$

An exceptionally large scatter results, even though all data are from one type of joint (double lap or double strap butt joint). This is partially due to different mean stress levels applied in the test. Taras and Greiner [13] propose the following correction for mean stress of riveted joints based on a curve fit of a relationship in the recommendation [42].

^b Column gives e if $n_{row} = 1$ or p if $n_{row} > 1$.

 $^{^{\}rm c}$ RLP = Red Lead Paint or similar coating.

^d Six tests included in [20], but two duplicate with [31].

^e Erroneously reported as without RLL in [34].

 $^{^{\}rm f}$ Measured tensile strength not reported. Steel grade S355 for [41] and St37 or similar for other sources.

^g Some tests in [18] are with drilled-out rivets. Tests where an entire row of rivets is drilled out are considered where n_{row} refers to the remaining rows. Tests where individual rivets in a row are drilled out are abandoned.

h Tests with reduced clamping force.

ⁱ Tests part of current study; not reported elsewhere.

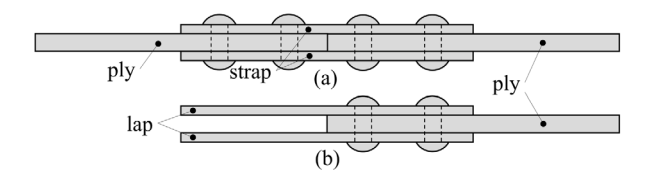


Fig. 2. Double covered joints: (a) Double strap butt joint; (b) Double lap joint. We treat these as one group.

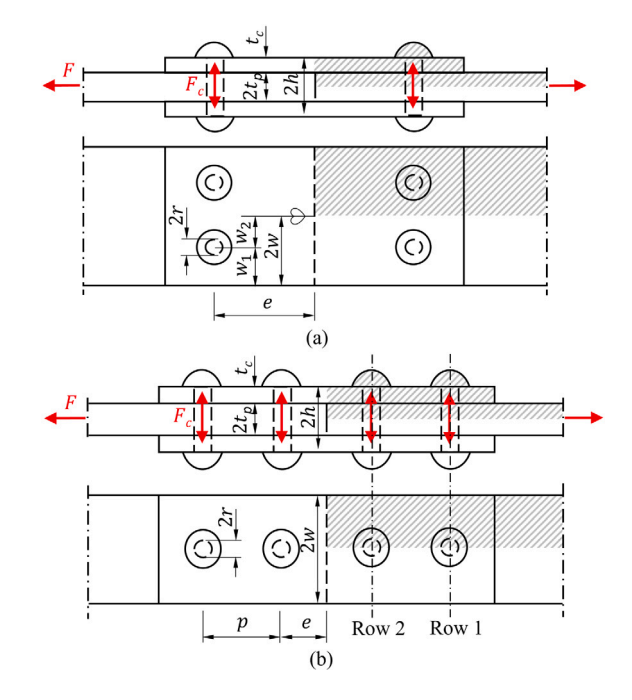


Fig. 3. Definition of joint geometry: (a) Joint with $n_{row}=1$ and $n_{pr}=2$; (b) Joint with $n_{row}=2$ and $n_{pr}=1$. The hatched area indicates the part modelled with the FE method.

This correction is also used elsewhere [16,33]:

$$f_R = \begin{cases} \frac{1-R}{1-0.6R} & \text{if } 0 \le R < 1\\ \frac{1-R}{1-0.4R} & \text{if } R < 0 \end{cases}$$
 (2)

where stress ratio R is the ratio between minimum and maximum stress of the cycle, σ_{net}^{min} and σ_{net}^{max} , respectively:

$$R = \frac{\sigma_{net}^{min}}{\sigma_{net}^{max}} \tag{3}$$

Fig. 4(b) provides the data corrected for the stress ratio. The scatter reduces compared to subfigure (a), however, it is still excessively large. Fitting the failed data with a Basquin relation:

$$\log_{10}(N) = C + m \log_{10}(\Delta \sigma_{net}) \tag{4}$$

and assuming a slope parameter m = -5, the standard deviation of the log-life parameter C is $\mathbb{S}(C) = 0.44$.

The left-hand graphs of Fig. 5 show the data of the failed specimens distinguishing different geometric and material parameters (right-hand graphs will be introduced later). The lines in the graphs indicate the mean Basquin relation of the subsets, in all cases ignoring run-outs. Fig. 5(a) demonstrates that the clamping stress (normal or low) and the surface condition (mill scale or RLP) has important influence on the fatigue resistance. The number of rivet rows n_{row} and the plate width relative to the hole radius also noteworthy influence the resistance, Fig. 5(b) and (c), respectively. Smaller but non-negligible influence stems from the semi grip relative to the hole radius, Fig. 5(d). The

data also suggest an influence of the ply tensile strength, Fig. 5(e). We conclude that the net section stress does not well capture the influence of specimen geometry. Our hypothesis is that the hoop stress at the hole edge in the plate correlates better with the fatigue resistance. To estimate the hoop stress, we developed analytical closed-form equations. These equations are based on the theory of applied mechanics and on results of FE simulations. Sections 3 and 4 describe the FE model and the analytical model, respectively.

3. FE model

Imam et al. [27,43] have developed a FE modelling method of hot riveted joints aimed at determining the stress distribution in the plates. Jesus et al. [14,44] refined their method. Since then, others [45-47] have applied similar models, and it is also applied here. This section gives a brief description. The joints are modelled in the FE software Abagus 2020 HF2. The geometry of the plates and the rivets is modelled with type C3D20R solid elements, having quadratic shape function and reduced integration scheme. Making use of symmetry, only one eight of the geometry is modelled according to the hashed area in Fig. 3 and symmetry boundary conditions are applied at the symmetry planes. The rivet head geometry is taken from [48]. The rivets are placed centrally in the holes and the rivet shaft radius is taken equal to the hole diameter. Ten elements are applied around a quarter of the circumference of the hole, and five elements are applied in the thickness direction of the ply. Fig. 6 gives an impression of the mesh size. Various models are made with different geometric parameters n_{row} , n_{pr} , r/w, h/r and t_p/t_s .

Linear elastic material with Young's modulus $E=210\,000\,$ MPa and Poisson ratio v=0.3 is applied for the solid elements. Contact interactions are applied between all plates and between plates and rivets, with a penalty model applied in normal direction and a Coulomb friction model applied in tangential direction. The friction coefficient is taken as $\mu_{ms}=0.3$ for the simulations with plate-to-plate contact, which is representative of mill scale contact according to measurements in [49]. Based on measurements with red lead painted plates [49], a friction coefficient of $\mu_{rlp}=0.05$ is applied between the plate faces in the RLP simulations, but the coefficient is taken as μ_{ms} between the rivet and the plates because RLP appears absent at these contacts, see Fig. 7. Additional simulations are conducted with a friction coefficient of 0.06 or (almost) 0 at all interactions to study the effect on friction.

The FE simulations consist of three steps:

- 1. The initial clamping stress in the rivets, $\sigma_{cl,0}$, is applied by assigning a coefficient of linear thermal expansion to the rivet shaft and applying an imposed temperature to it. The resulting contraction causes rivet clamping and it causes a small clearance between the rivet and the hole. The temperature is determined by trial to arrive at the desired clamping stress.
- The maximum external load is stepwise applied. The node giving the highest principal stress in the ply is selected and the hoop stress of that node is recorded.
- 3. The minimum external load is stepwise applied. The hoop stress of the node selected in Step 2 is recorded.

The stress range is determined by subtracting the hoop stress of Step 3 from that of Step 2. The unloading step (Step 3) is necessary because friction causes non-linear behaviour and consequently, unloading causes another stress distribution in the plates than loading. Simulations with Steps 2 and 3 repeated multiple times showed that the maximum stress range does not change after the first cycle. We verified in a number of simulations that the node selected in Step 2 based on the maximum principal stress is indeed the node with the largest hoop stress range. This node is always located at the hole edge of the first rivet row, close to the net section location.

The solid curves in Fig. 8 give the hoop stress as a function of the applied net section stress resulting from a selection of the simulations

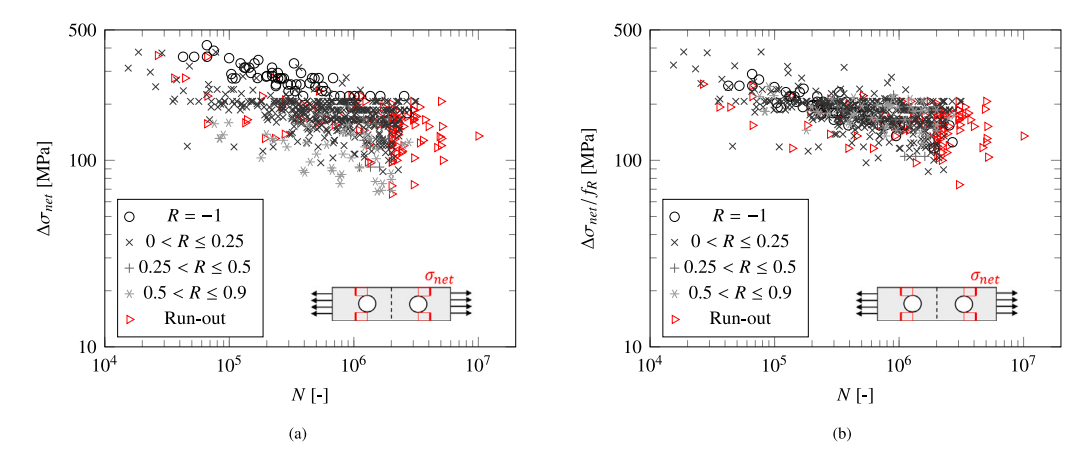


Fig. 4. Fatigue test data evaluated with the net section stress range: (a) As published; (b) After correction for mean stress.

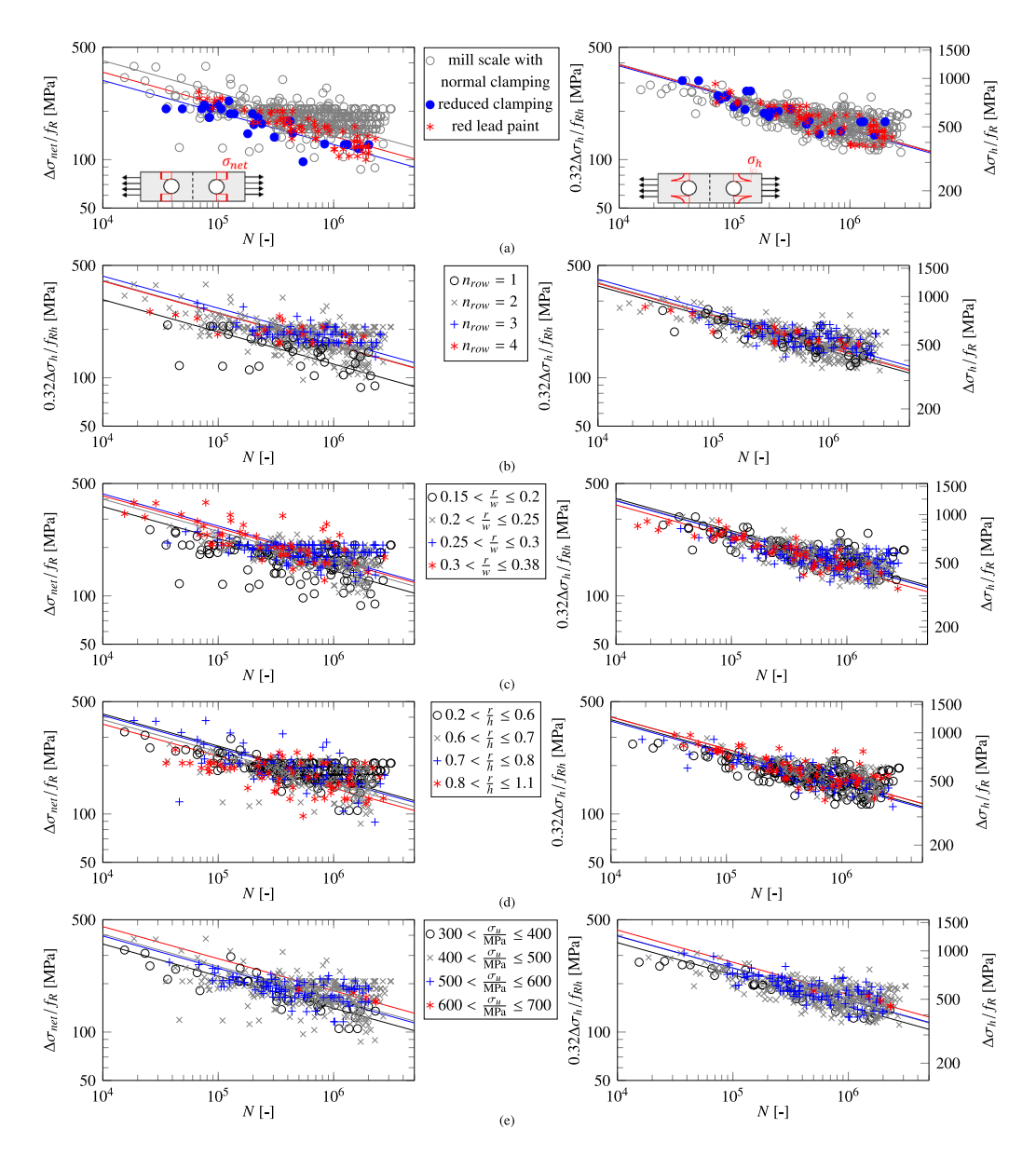


Fig. 5. Subsets of fatigue test data corrected for mean stress, with net section stress range (Eq. (1)) on the left and hoop stress range on the right (Eqs. (5)–(37), with $\sigma_{cl,0}$ according to Eq. (38) or $\sigma_{cl,0}=0$ in case of reduced clamping, $\mu_{ms}=0.33$, and $\mu_{rlp}=0.06$): (a) Clamping; (b) Number of rivet rows; (c) Rivet diameter over plate width; (d) Ply thickness over rivet diameter; (e) Ply tensile strength. The difference between the geometrical subsets reduces when using the hoop stress range.

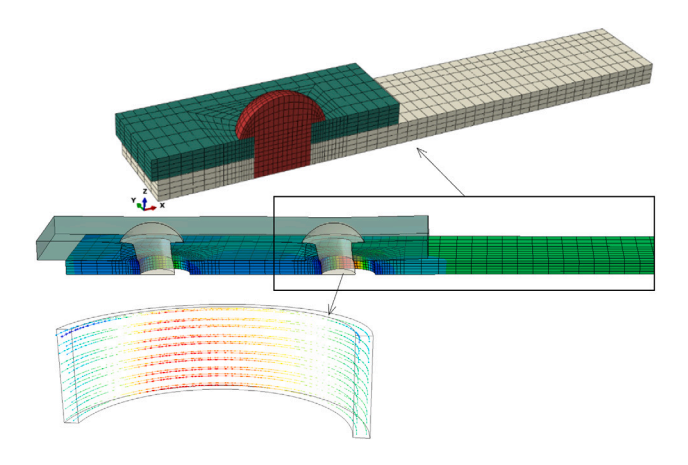


Fig. 6. Example of a FE model with $n_{row} = 2$ and $n_{pr} = 1$, with the top picture showing the mesh, the centre picture showing the stress distribution in the ply (red = high stress, blue = low stress) and the bottom figure showing the hoop stress around the hole of the first (decisive) rivet row.



Fig. 7. Disassembled RLP joint taken from a bridge in The Netherlands, showing no RLP remnants on the rivet shaft and under the rivet head.

(dashed curves will be introduced later). Subfigure (a) gives the results of simulations with the same geometry but with different friction coefficients. A larger friction coefficient between the rivet and the plates increases the hoop stress at maximum load. A larger friction coefficient between the plates increases the hoop stress at minimum load, thereby reducing the stress range. The insertion shows the hole deformation in lateral direction at high load. Subfigure (b) gives the results of three simulations of different geometries with mill scale friction ($\mu_{ms}=0.3$), all loaded with R=-1 and a gross section stress range of 300 MPa. The subfigure shows a significant difference between the hoop stress and the net section stress for the three cases. This relation appears non-linear, with the behaviour under compression being different from tension. This also implies that the hoop stress ratio R_h differs from the net section stress ratio R.

4. Analytical model

4.1. Lay-out of the model

The FE method enables to determine the linear elastic hoop stress, but it requires detailed modelling, can be subject to user interpretation, is computationally expensive, and therefore not suited for practical assessment of bridges. For this reason, we developed an analytical model to estimate the hoop stress, consisting of six steps visualised in Fig. 9:

- 1. Estimate the load transfer by each rivet using a spring system.
- 2. Estimate the rivet clamping stress and the associated stress in the ply.
- 3. Estimate the part of the load transferred by friction.
- 4. Determine the stress concentration factor (SCF) for the hoop stress of a plate with a hole and of a plate loaded by a pin.
- 5. Estimate the hoop stress at maximum load from Steps 1-4.

6. Estimate the hoop stress at minimum load from Steps 1-4.

Stress range and mean stress follow from Steps 5 and 6. We have developed predecessors of this model for rivets with $n_{row}=2$ [34] and snug-tight bolted joints [50]; the model is extended here to cover a wide range of geometries and load conditions. The steps are elaborated hereafter for the cases with and without friction. For convenience, we have developed a Microsoft Excel sheet with Visual Basic application as well as a Python script incorporating the model and made it available as supplementary material, see Appendix A.

4.2. Model without friction

The elaboration of the steps for the special case without friction between the plates and between the plates and rivets is as follows.

Step 1. A quarter of the geometry is considered (one joint side, semi thickness, full width). Each rivet and each plate in between the rivets is modelled as a spring:

$$F = ku \tag{5}$$

where F is the force vector, u is the displacement vector in load direction and k is the spring stiffness matrix. Fig. 9(a) shows the spring system for $n_{row} = 2$ and $n_{pr} = 1$:

$$\begin{bmatrix} F/2 \\ 0 \\ 0 \\ -F/2 \end{bmatrix} = \begin{bmatrix} k_p + k_r & -k_p & -k_r & 0 \\ -k_p & k_p + k_r & 0 & -k_r \\ -k_r & 0 & k_s + k_r & -k_s \\ 0 & -k_r & -k_s & k_s + k_r \end{bmatrix} \begin{bmatrix} u_{1,p} \\ u_{2,p} \\ u_{1,s} \\ 0 \end{bmatrix}$$
(6)

The system can easily be extended to other values of n_{row} and n_{pr} . For convenience, we characterise each spring by its compliance 1/k. FE simulations of joints with a single rivet are employed to obtain the compliances. Analytical descriptions in [51–54] are compared to these compliances and modifications are applied to some descriptions to better resemble the stiffness values following from the FE models. We decompose the ply and strap compliances in two parts, namely, in between rivet holes with length p-2r and at the rivet hole with length 2r.

$$\frac{1}{k_p} = \frac{p - 2r}{2wt_p E} + \frac{2r}{2(w - r)t_p E} \tag{7}$$

$$\frac{1}{k_s} = \frac{p - 2r}{2wt_s E} + \frac{2r}{2(w - r)t_s E} \tag{8}$$

Using the derivation in [54] but modifying it for double covered joints, we derived equations for rivet bending and rivet shear deformations between the ply and strap midplanes. We took the equations for bearing deformation at the hole in the ply from [51]. The bearing deformation of the rivet appeared half of the latter value. The rivet stiffness then follows from:

$$\frac{1}{k_r} = \frac{9t_s^3 + 48t_s^2t_p + 64t_st_p^2 + 16t_p^3}{96E\pi r^4} + \frac{4t_p + 3t_s}{8aG\pi r^2} + \frac{1}{t_pE} + \frac{1}{t_sE} + \frac{1}{2t_pE}$$
 (9)

$$a = \frac{6(\nu+1)^2}{4\nu^2 + 12\nu + 7}$$

where G = E/(2[1 + v]) is the shear modulus, a accounts for the non-uniform strain over the cross section [55], and the subsequent terms in Eq. (9) refer to rivet bending, rivet shear, ply bearing, strap bearing and rivet bearing. The force fraction taken by rivet row i follows from:

$$f_i = 2k_r(u_{i,p} - u_{i,s})n_{pr}/F (10)$$

The force fractions per rivet row reduce as the number of rows increases. This is the main cause of the increased fatigue resistance with increasing number of rivet rows in the left-hand graph of Fig. 5(b).

Step 2. The rivet clamping stress causes a compressive stress in thickness direction of the ply. We approximate the clamping stress as

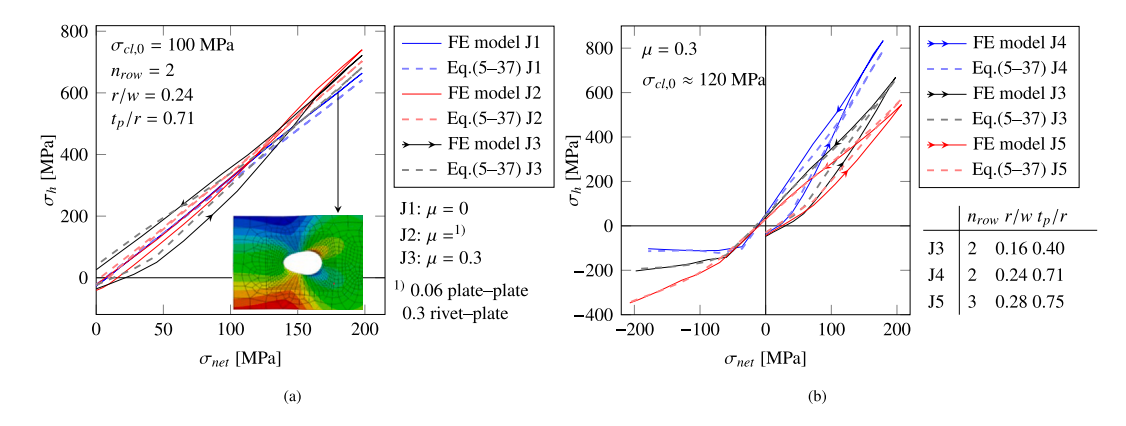


Fig. 8. Hoop stress for example cases with the FE model (solid) and the analytical model (dashed): (a) Effect of μ (same geometry, R=0) (b) Effect of geometry ($\mu=0.3$, R=-1). The hoop stress over net stress ratio depends on μ and on the geometry. This ratio is different in tension as in compression. The figure shows good agreement between the analytical model and the FE model.

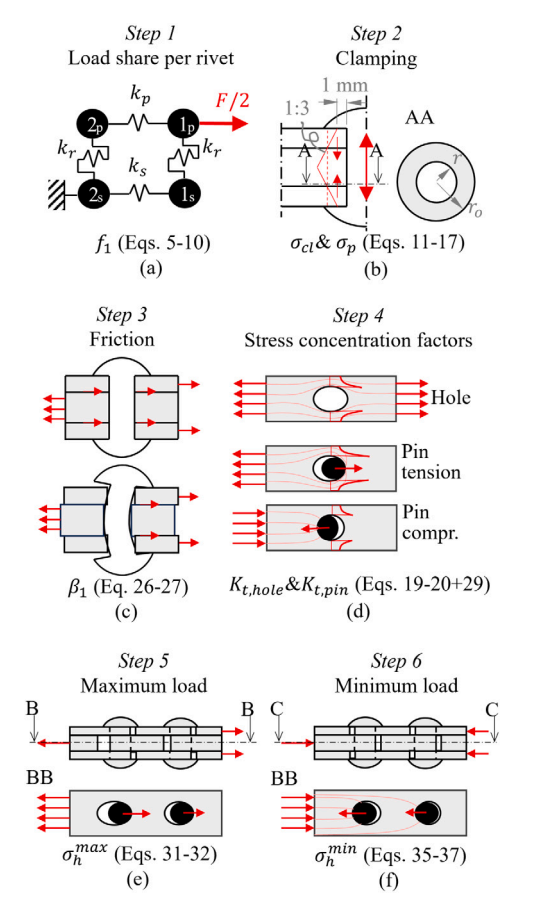


Fig. 9. Steps 1-6 (subfigures a-f) with associated equations comprising the analytical model.

being transferred in the ply through a cone with inner radius r and outer radius r_o , see 9(b):

$$r_o = 1.1r + h/3 \tag{11}$$

where the factor of 3 is a load spread factor [56] and 1.1r is an estimate of the load carrying radius of the rivet head.

Upon loading the joint, the Poisson effect of the ply (and straps) influences the clamping stress σ_{cl} , which hence differs from the initial clamping stress $\sigma_{cl,0}$. The average stress in the ply just before the first rivet row is equal to σ_{net} , causing a contraction in thickness direction

of:

$$\Delta u_z = t_p v \sigma_{net} / E \tag{12}$$

The stress in the straps is close to zero at that location. The ply contraction reduces the clamping stress to the ratio of the rivet stiffness and the ply stiffness in thickness direction. The rivet and ply can be modelled as springs in thickness direction, with the following respective stiffness values:

$$k_{r,z} = \frac{2\pi E}{h} r^2 \tag{13}$$

$$k_{p,z} = \frac{2\pi E}{h} (r_o^2 - r^2) \tag{14}$$

The resulting deformation of the rivet is:

$$\Delta u_{r,z} = \Delta u_z \frac{k_{p,z}}{k_{r,z} + k_{p,z}} \tag{15}$$

Hence the rivet clamping stress is:

$$\sigma_{cl} = \max\left(0, \sigma_{cl,0} - \nu \sigma_{net} \frac{t_p}{h} \frac{r_o^2 - r^2}{r_o^2}\right)$$
 (16)

The ply stress in thickness direction near the hole caused by clamping is equal to $\sigma_{cl}r^2/(r_o^2-r^2)$. Assuming expansion can freely occur in the hole radial direction but is fully restrained in tangential direction, a hoop stress (preload stress) σ_p results because of clamping:

$$\sigma_p = -\sigma_{cl} \frac{r^2}{r_o^2 - r^2} \frac{\nu(1 - \nu)}{(1 + \nu)(1 - 2\nu)} \tag{17}$$

Step 3. The consideration of the frictional force distribution is obsolete for the special case without friction.

Step 4. In joints with $n_{row} > 1$, the first rivet row transfers a certain fraction of the load through pin action and another fraction bypasses the hole and is transferred at subsequent rivet rows. The two types of loading cause different stress concentrations. Each SCF given below refers to the net section:

$$K_t = \sigma_h / \sigma_{net} \tag{18}$$

The SCF of a plate with a hole is taken as the plane stress solution of [57]:

$$K_{t,hole} = 2 + \left(1 - \frac{r}{w}\right)^3$$
 (19)

The maximum stress at the hole in a plate with finite thickness is slightly higher than the plane stress solution, whereas the stress at the plate surface is lower [58]. The plane stress solution is a reasonable approximation for the location at which the (hole and pin) combined SCF is maximum.

The SCF for pin loading depends on the degree of hole filling, the flexibility of the rivet and the ligament in front of the rivet (p for $n_{row} \ge$

1 and e or > e for $n_{row} = 1$ in tension or compression, respectively). We obtained the SCF for pin loading by fitting of the results of the FE model of Section 3, using one rivet without clamping and without friction. If loaded in tension, the load first bypasses the hole before it is transferred to the rivet, see the centre picture in Fig. 9(d). In case of compressive loading, the rivet is squeezed between the ply and the straps. Consequently, it expands in the joint width direction and thereby it presses against the hole edge, causing a *tensile* hoop stress and thereby a *negative* SCF. This effect is responsible for the lower hoop stress in compression as compared to tension in Fig. 8(b) and it causes the large required stress ratio correction for negative stress ratios in Eq. (3). Further, the stress does not bypass the hole if loaded in compression, see the bottom picture in Fig. 9(d). A conservative estimate for the SCF is obtained as the SCF for the hole minus the SCF for pin loading in tension:

$$K_{t,pin} = \begin{cases} a_1 \left(\frac{r}{w}\right)^{b_1} & \text{if } \sigma_{net} \ge 0 \land n_{row} = 1\\ a_2 \left(\frac{r}{w}\right)^{b_2} & \text{if } \sigma_{net} \ge 0 \land n_{row} > 1\\ K_{t,hole} - a_2 \left(\frac{r}{w}\right)^{b_2} & \text{if } \sigma_{net} < 0 \end{cases}$$

$$(20)$$

$$a_1 = 1.517 - 0.307 \left(\frac{t_p}{r}\right) + 0.266 \left(\frac{t_p}{r}\right)^2$$

$$b_1 = -0.820 + 0.039 \left(\frac{t_p}{r}\right) - 0.042 \left(\frac{t_p}{r}\right)^2$$

$$a_2 = 1.171 - 0.170 \left(\frac{t_p}{\pi}\right) + 0.147 \left(\frac{t_p}{\pi}\right)^2$$

$$b_2 = -0.944 + 0.070 \left(\frac{t_p}{r}\right) - 0.064 \left(\frac{t_p}{r}\right)^2$$

The equation is valid for the range $0.1 \le r/w \le 0.5$ and $0.25 \le t_p/r \le 2.0$. The difference between the solutions for one and for multiple rows in tension is the distance between the rivet and the end of the ply. The equation for $n_{row}=1$ is an approximation, because it is based on a fit of FE data with e/w=1.0 whereas 0.6 < e/w < 2 for the tested joints with $n_{row}=1$. The equation for multiple rows and/or compression is also determined from simulations with one row, but with e/r=5, representing a large distance between the first rivet row and the ply end. The end effect is negligible in this case. We have verified with the FE method that the SCF for pin loading is also valid for $n_{pr}>1$.

Step 5. In joints with multiple rows, the hoop stress in the ply is highest at the first rivet row, because the load fraction transferred by that row and the load fraction bypassing it is higher than at subsequent rows, Fig. 9(e). This observation from the analytical model is consistent with the location of fatigue failure in the tests. The SCF of rivets in the first row can be estimated with:

$$K_{t,1} = f_1 K_{t,pin} + (1 - f_1) K_{t,hole}$$
(21)

where f_1 follows from Eq. (10). Whereas $K_{t,hole}$ decreases with decreasing r/w, $K_{t,pin}$ increases with decreasing r/w. The interaction determines the influence of r/w on the fatigue resistance, where $K_{t,pin}$ dominates in joints with a small number of rows and causes the relatively low fatigue resistance of joints with low r/w in Fig. 5(c). The hoop stress at maximum load is:

$$\sigma_h^{max} = K_{t,1}^{max} \sigma_{net}^{max} + \sigma_p^{max} \tag{22}$$

where σ_p^{max} and $K_{t,1}^{max}$ follow from Eqs. (17) and (21) at maximum load. Step 6. In the special case without friction, the hoop stress during unloading follows the same path as during loading (and can hence be determined in a similar way as Eq. (22)). In case of compression, $K_{t,1}^{min}$ at minimum load may be negative. The minimum stress of the range then occurs at the tipping point, where $K_{t,1}^{min} = 0$, see Fig. 10:

$$\sigma_h^{min} = \begin{cases} \sigma_p^t & \text{if } K_{t,1}^{min} < 0\\ K_{t,1}^{min} \sigma_{net}^{min} + \sigma_p^{min} & \text{if } K_{t,1}^{min} \ge 0 \end{cases}$$
 (23)

where σ_p^t follows from Eq. (17) at the tipping point, in the case without friction occurring at an applied stress $\sigma_{net} = 0$.

4.3. Model with friction

The general case with friction requires modifications of the model. It involves a larger number of fits of the FE data. The equations in this section reduce to those of Section 4.2 if the friction coefficient $\mu = 0$.

Step 1. Friction changes the load distribution between rivet rows at low load levels. It is possible but complex to consider this in the analytical model, see Step 3. Simulations with the FE method show that the effect of friction on f_1 is smaller than 10% if the applied load is larger than 1.6 times the total slip force: $F^{max} > 1.6 n_{row} n_{pr} F_{slip}$, where:

$$F_{slip} = 2\mu \sigma_{cl} \pi r^2 \tag{24}$$

where μ is either μ_{ms} or μ_{rlp} depending on the plate contact in the specimen. All collected tests satisfy this criterion. Eqs. (5)–(10) are therefore also applied for the case with friction as a reasonable approximation.

Step 2. This step is equal to that of the model without friction.

Step 3. We define a bearing ratio ranging between 0 and 1 for the entire load being transferred through friction or bearing, respectively:

$$\beta_i = \max\left(0, \frac{|F_i| - F_{slip}}{|F_i|}\right) \tag{25}$$

where F_i is the load at rivet row *i*. For a rivet in the first rivet row, Eq. (25) can be written as:

$$\beta_1 = \max\left(0, \frac{|f_1\sigma_{net}| - \sigma_{slip}}{|f_1\sigma_{net}|}\right) \tag{26}$$

where

$$\sigma_{slip} = \frac{\mu \sigma_{cl} \pi r^2}{t_p(2w - 2r)} \tag{27}$$

with σ_{cl} according to Eq. (16). The bearing ratio β_1 needs to be determined at maximum and at minimum load.

Note that the rivet spring stiffness in Step 1 also changes due to friction, giving a rivet spring stiffness of k_r/β_i with k_r according to Eq. (9). However, this would imply a complex set of equations because k_r/β_i determines f_i which in turn determines β_i . As explained above, ignoring the effect of friction in the spring model gives a reasonably accurate load fraction estimate.

Step 4. The SCF of a single rivet follows from:

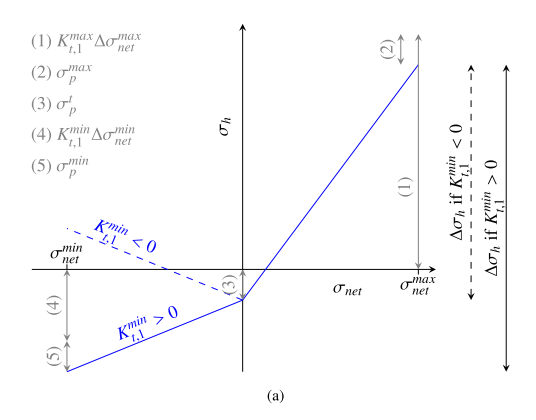
$$K_{t,s} = \beta_1 K_{t,pin,\mu} + (1 - \beta_1) K_{t,fric}$$
(28)

where $K_{t,fric}$ is the SCF for friction and $K_{t,pin,\mu}$ is a modified SCF for pin loading, as follows. Contact between the rivet shank and the hole edge occurs around half of the rivet perimeter at high load levels, see the insertion in Fig. 8(a). Friction at that contact location increases the hoop stress, which depends on the friction coefficient, contact area, and bearing ratio. We incorporate this effect in the SCF for pin loading:

$$K_{t,pin,\mu} = \begin{cases} K_{t,pin} + 2\mu_{ms} & \text{if } \sigma_{net} \ge 0\\ K_{t,pin} - 2\mu_{ms} & \text{if } \sigma_{net} < 0 \end{cases}$$
 (29)

where the factor 2 follows from a fit of the FE results and $K_{t,pin}$ follows from Eq. (20).

Next, the SCF for friction needs to be determined. The rivet maintains its shape at low bearing ratios ($\beta \approx 0$). Approximately half of the friction force is then transferred before the hole and the other half bypasses the hole, resulting in a SCF of $K_{t,hole}/2$. The rivet bends at high bearing ratios, see the right graphic of Fig. 9(c). If loaded in tension, prying of the bended rivet causes rivet head to plate contact to be established behind the rivet hole, resulting in the SCF for pin loading. In case of compression, prying causes frictional force transfer before the hole and hence no stress at the hole. A quadratic transition between



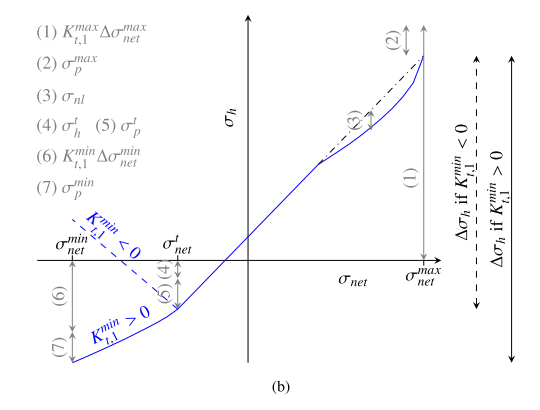


Fig. 10. Schematic hoop stress description during unloading, explaining the terms in Eqs. (23) and (35): (a) without friction, Eq. (23); (b) with friction, Eq. (35).

the two cases with respect to β gives a reasonable match with the FE method:

$$K_{t,fric} = \begin{cases} (1 - \beta_1^2) K_{t,hole} / 2 + \beta_1^2 K_{t,pin,\mu} & \text{if } \sigma_{net} \ge 0\\ (1 - \beta_1^2) K_{t,hole} / 2 & \text{if } \sigma_{net} < 0 \end{cases}$$
(30)

Step 5. Equivalent to Eq. (18) and making use of Eq. (28)–(30), the SCF in the loading stage is:

$$K_{t,1,\mu} = f_1 K_{t,s} + (1 - f_1) K_{t,hole}$$
(31)

The maximum hoop stress is:

$$\sigma_h^{max} = K_{t,1,\mu}^{max} \sigma_{net}^{max} + \sigma_p^{max} \tag{32}$$

with σ_n^{max} according to Eq. (17).

Step 6. FE simulations with a single rivet indicate that the hoop stress at unloading is equal to 0 if the net section stress is equal to -3/4 times the slip stress. The hoop stress follows a slightly non-linear unloading path between maximum stress (Eq. (32)) and the slip stress in compression. For a joint with a single rivet:

$$\sigma_{h,s}^{min} = \sigma_p^{min} - \sigma_{nl} + \left(K_{t,1,\mu}^{max} \sigma_{net}^{max} + \sigma_{nl} \right) \frac{\sigma_{net}^{min} + 3/4 \sigma_{slip}^{min}}{\sigma_{net}^{max} + 3/4 \sigma_{slip}^{min}}$$

$$\text{if } \sigma_{net}^{min} \ge -\sigma_{slin}^{min}$$
(33)

where σ_{nl} is a fit accounting for the non-linearity of the unloading path, see Fig. 10:

$$\sigma_{nl} = \mu \beta_1^{min} K_{t,1,u}^{min} \sigma_{net}^{min} \tag{34}$$

If loaded in compression, the part of the net section stress beyond the slip stress is multiplied with $K_{t,1,\mu}^{min}$. Combining this with Eq. (33) and extending it to multiple rivet rows gives:

$$\sigma_h^{min} = \begin{cases} \text{Case 1} & \text{if } \sigma_{net}^{min} \geq \sigma_{net}^t \\ \text{Case 2} & \text{if } \sigma_{net}^{min} < \sigma_{net}^t \land K_{t,1,\mu}^{min} \geq 0 \\ \text{Case 3} & \text{if } \sigma_{net}^{min} < \sigma_{net}^t \land K_{t,1,\mu}^{min} < 0 \end{cases}$$

$$(35)$$

Case
$$1 = \sigma_p^{min} + \sigma_h^t - \sigma_{nl} + \left(K_{t,1,\mu}^{max}\sigma_{net}^{max} - \sigma_h^t + \sigma_{nl}\right) \frac{\sigma_{net}^{min} - \sigma_{net}^t}{\sigma_{net}^{max} - \sigma_{net}^t}$$

Case
$$2 = \sigma_p^{min} + \sigma_h^t + K_{t,1,\mu}^{min} \left(\sigma_{net}^{min} - \sigma_{net}^t\right)$$

Case $3 = \sigma_n^t + \sigma_h^t$

where σ_{net}^t and σ_n^t are the net section stress and the hoop stress, respectively, at the tipping point, see Fig. 10. The tipping point can be found by incrementally lowering the applied stress and determining the corresponding slip stress, until these two values equate. However, the slip stress at minimum load forms a good approximation and is easier to obtain:

$$\sigma_{net}^t \approx -\sigma_{slip}^{min}/f_1 \tag{36}$$

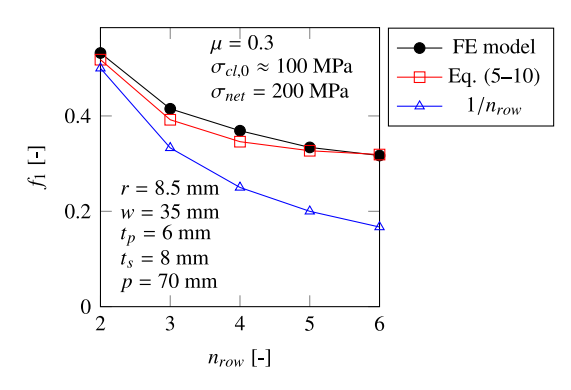


Fig. 11. Load fraction transferred at the first rivet row f_1 for example joints with different row numbers. The analytical model of Eq. (5)–(10) agrees well with the FE models. The load fraction f_1 is larger than an equal fraction per rivet (=1/ n_{row}).

Similarly, the prestress at the tipping point can be approximated at minimum stress: $\sigma_p^t \approx \sigma_p^{min}$. The tipping point hoop stress follows from:

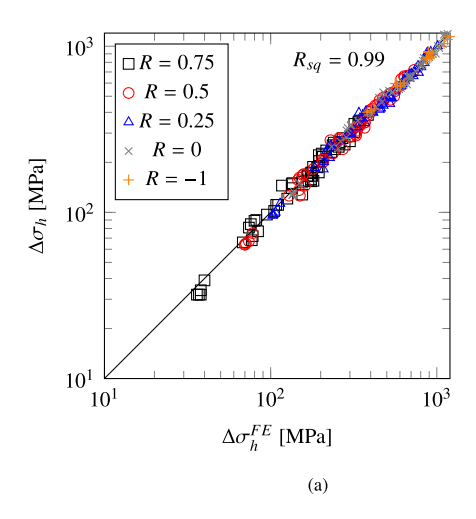
$$\sigma_{h}^{t} = (1 - f_{1})K_{t,hole}\sigma_{net}^{t} + \left[K_{t,1,\mu}^{max} - (1 - f_{1})K_{t,hole}\right] \frac{\sigma_{net}^{max}\sigma_{net}^{t}}{4\sigma_{net}^{max} - 3\sigma_{net}^{t}}$$
(37)

The basic inputs of the analytical model are hence f_1 , σ_{cl} , σ_p , $K_{t,hole}$, $K_{t,pin,\mu}$ and σ_{nl} .

4.4. Model performance

As a representative example of the performance of the spring model, Fig. 11 gives the load fraction transferred at the first rivet row according to the spring model and the FE simulations of joints with two up to six rivet rows. The fraction resulting from the spring model agrees reasonable with that according to the FE simulations. The figure also provides the fraction if assuming an equal share per rivet row, demonstrating that the first row takes a larger share than average.

The dashed curves in Fig. 8 present the analytical model prediction for the example cases. The figure shows a good agreement with the FE models. A total of 500 FE simulations are conducted with different geometries and loads, ranging between $1 \leq n_{row} \leq 6$, $1 \leq n_{pr} \leq 3$, $0 \leq \mu \leq 0.3$, $0.16 \leq r/w \leq 0.31$, $0.47 \leq t_p/r \leq 0.8$, $1 \leq t_s/t_p \leq 1.7$, 80 MPa $\leq \sigma_{cl} \leq 130$ MPa, 50 MPa $\leq \sigma_{net}^{max} \leq 200$ MPa and $-1 \leq R \leq 0.75$. Fig. 12 compares the hoop stress range $\Delta \sigma_h = \sigma_h^{max} - \sigma_h^{min}$ and the mean stress $\overline{\sigma}_h = (\sigma_h^{max} + \sigma_h^{min})/2$ of the analytical model with that of the FE models for all simulations, where superscript FE refers to the FE models. The figure shows a good agreement. The coefficient of determination is $R_{sq} = 0.99$ for both parameters. The mean of the ratios $\Delta \sigma_h/\Delta \sigma_h^{FE}$ is 0.99 and the standard deviation is 0.06. The mean of the ratios $\overline{\sigma}_h/\overline{\sigma}_h^{FE}$ is 1.01 and the standard deviation is 0.06. We consider



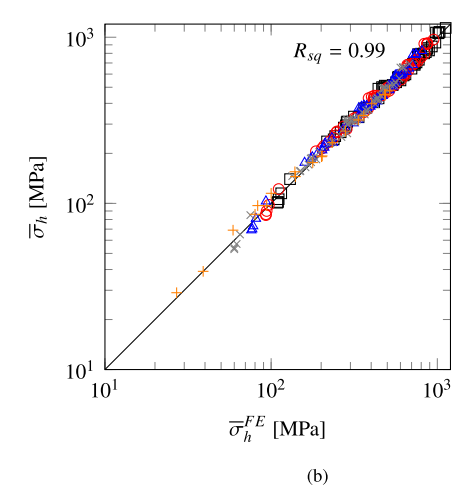


Fig. 12. Prediction accuracy of the analytical model compared to the FE models: (a) Hoop stress range; (b) Mean hoop stress. The two models agree well, with a coefficient of determination of $R_{sq} = 0.99$ for both parameters.

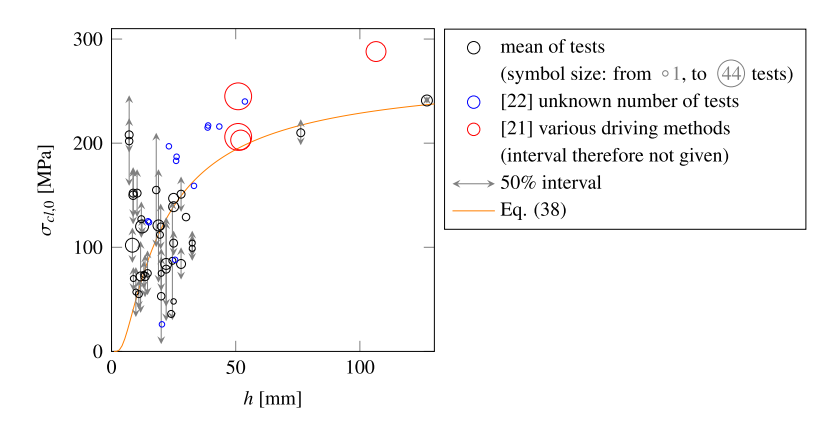


Fig. 13. Initial clamping stress versus semi grip, data from [18,21,22,24,59–63]. The larger the grip, the larger is the mean clamping stress and the smaller is the scatter in clamping stress.

the analytical model suited for estimating the hoop stress of the fatigue

5. Results

This section describes the evaluation of the test database with the hoop stress according to the analytical model. The mean friction coefficient of $\mu_{ms}=0.33$ according to [49] is applied in the analyses of specimens without RLP. Based on the same source, the friction coefficient is taken as $\mu_{rlp}=0.06$ for plate–plate contact (Eq. (27)) and $\mu_{ms}=0.33$ (Eq. (29)) for rivet–plate contact in the analyses of specimens with RLP. Various authors measured the initial clamping stress in rivets [18,21,22,24,59–63]. Fig. 13 shows the collected data. The initial clamping stress increases with increasing grip, but the scatter is significant. We fitted an exponential function through the collected data and used the average value of $\sigma_{cl,0}$ in the analyses of the fatigue tests with normal clamping:

$$\sigma_{cl,0} = \frac{265 \text{ MPa}}{\exp\left(\frac{12 \text{ mm}}{h}\right)} \tag{38}$$

We took the clamping stress as $\sigma_{cl,0}=0$ in the analyses of tests with reduced clamping. To enable a comparison of the fatigue test data evaluated with the linear elastic hoop stress and with the net section stress, the hoop stress range is multiplied with 0.32, which is the inverse mean of the SCF of all tests.

Fig. 14(a) gives the fatigue lives of the test database as a function of the hoop stress range on the right ordinate, and 0.32 times the hoop

stress range on the left ordinate. Similar to the net section stress, a stress ratio correction factor is applied that is calibrated with the data:

$$f_{Rh} = \frac{1 - R_h}{1 - 0.9 R_h} \tag{39}$$

$$R_h = \sigma_h^{min} / \sigma_h^{max} \tag{40}$$

A differentiation between R < 0 and $R \ge 0$ as for the net section stress in Eq. (2) is not necessary. Note that many other stress ratio corrections are available. We chose Eq. (39) for its simplicity, not because it gives the best fit to the data. Figs. 14(b) gives the fatigue lives as a function of the stress ratio corrected hoop stress (blue arrows will be introduced later). Comparing Figs. 4 and 14, the scatter in the fatigue life reduces significantly if evaluated with the hoop stress instead of the net section stress.

The analytical model of Section 4 does not allow predicting the fatigue resistance using general material properties and a local approach such as the theory of critical distances [64]. Such methods can be applied to riveted joints [65], but they require the stress gradient, which is not part of the analytical model. Therefore, the fatigue resistance is determined through regression of the test data. Assuming a Basquin equation with an inverse slope parameter m = -5 and ignoring runouts, the standard deviation of C is $\mathbb{S}(C) = 0.33$ and it is $\mathbb{S}(C) = 0.31$ for a best fitting inverse slope of m = -4. This is substantially lower than the standard deviation evaluated with the net section stress range, see Table 2.

The right-hand graphs of Fig. 5 provide the data of distinguished subsets. Compared to the net section stress range, the difference in

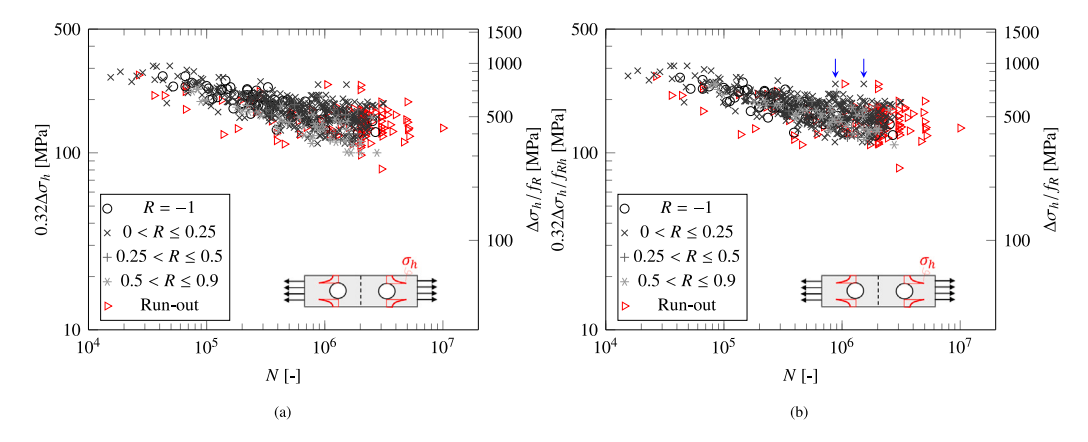


Fig. 14. Fatigue test data evaluated with the hoop stress range: (a) As published; (b) After correction for mean stress.

Table 2 Standard deviation of parameter C of the Basquin equation with an inverse slope m = -5, after stress ratio correction: $\mathbb{S}(C)$.

,	(-) -	
Subset	Net section stress	Hoop stress
All data	0.44	0.33
RLP	0.25	0.25
Mill scale, reduced clamping	0.28	0.25
Mill scale, normal clamping	0.43	0.34

fatigue resistance between the geometrical subsets reduces significantly when using the hoop stress. This demonstrates that the hoop stress better captures the fatigue-relevant effects of the geometric variability in riveted joints. The data suggest a positive correlation between the ply tensile strength and the fatigue life, but the number of data outside of the range 400 MPa < $\sigma_u \leq 600$ MPa is too small for a definite conclusion.

6. Discussion

6.1. Uncertainty of friction and clamping force

The scatter of the fatigue life is significantly smaller for the subset with RLP as compared to the subset of mill scale contact and normal clamping, see Table 2. The standard deviation of the RLP subset is similar to that of other notched components of similar steel grades and surface finish [50,66] and it can be considered as a typical value for the aleatory uncertainty in the fatigue life. Friction and clamping have a negligible influence on the hoop stress range of RLP specimens. The larger standard deviation of the mill scale contact subset is attributed to the aleatory uncertainties in clamping force and friction coefficient. To quantify the scatter in the S-N curve due to uncertainties in friction and clamping, we estimate their combined effect on the stress range of the specimens with mill scale contact and normal clamping. Based on [49,62], the standard deviations of $\sigma_{cl,0}$ and μ_{ms} are $\mathbb{S}(\sigma_{cl,0}) = 35$ MPa and $\mathbb{S}(\mu_{ms}) = 0.06$, respectively. Expectations $\mathbb{E}(\sigma_{cl.0})$ and $\mathbb{E}(\mu_{ms})$ are taken as in Section 5, i.e. given with Eq. (38) and equal to 0.33, respectively. Lognormal distributions are assumed for both variables. The two variables influence the slip stress σ_{slip} through multiplication. Their combined effect can be approximated with a lognormal distribution having the following parameters:

$$L_1 = \ln \left(\frac{\mathbb{E}(\sigma_{cl,0}) \mathbb{E}(\mu_{ms})}{\sqrt{b}} \right)$$
 (41)

$$b = 1 + \left[\mathbb{V}(\sigma_{cl,0})\right]^2 + \left[\mathbb{V}(\mu_{ms})\right]^2 + \left[\mathbb{V}(\sigma_{cl,0})\mathbb{V}(\mu_{ms})\right]^2$$

$$L_2 = \sqrt{\ln(b)} \tag{42}$$

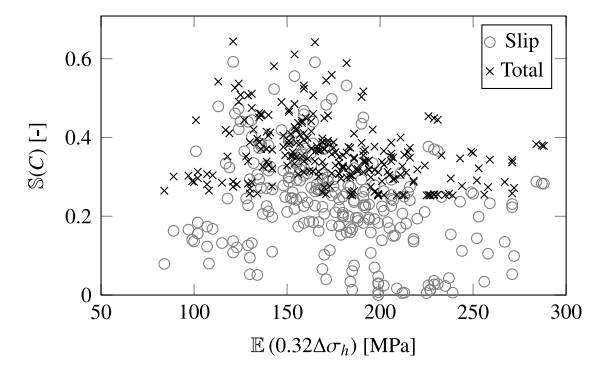


Fig. 15. Estimate of the standard deviation of the 10-th base logarithm of number of cycles, $\mathbb{S}(C)$, of the tests with mill scale contact, based on the uncertainty in slip force and the uncertainty in S–N curve of RLP data. The average of the estimated $\mathbb{S}(C)$ is 0.35, which agrees with the tests.

where $\mathbb V$ is the coefficient of variation. Using this distribution, we estimate the variation of slip force and subsequently the variation in the hoop stress range for each test using the model in Section 4. The standard deviation of the variation in hoop stress range averaged over all tests is 35 MPa. Assuming a Basquin equation with an inverse slope m=-5, the effect of the variation in hoop stress range can be translated to a variation in fatigue life. The grey circles in Fig. 15 provide the standard deviation of this variation, $\mathbb S(C_{slip})$ for each test with mill scale contact and normal clamping condition as a function of the expectation of the hoop stress $\mathbb E\left(0.32\Delta\sigma_h\right)$. The standard deviation of the total scatter of the fatigue life of these specimens can be estimated from $\mathbb S(C_{slip})$ and the standard deviation of the tests with RLP $\mathbb S(C_{rlp})$ (equal to 0.25 according to Table 2), as:

$$\mathbb{S}(C_{ms}) = \sqrt{\left(\mathbb{S}(C_{slip})\right)^2 + \left(\mathbb{S}(C_{rlp})\right)^2} \tag{43}$$

The black crosses in Fig. 15 provide the resulting estimate of the standard deviation of the total scatter in the fatigue life per test. The mean of this standard deviation over all tests is 0.36. This is almost equal to the actual scatter of the fatigue life of the specimens with mill scale contact: $\mathbb{S}(C) = 0.34$. The estimated standard deviation generally decreases for increasing stress range. This also agrees with the actual scatter, Fig. 14(b). The implication is that aleatory uncertainties are largely responsible for the scatter in fatigue life of the specimens with mill scale contact, and further optimization of the analytical model of Section 4 is not expected to cause a further major reduction in the scatter of the fatigue life prediction.

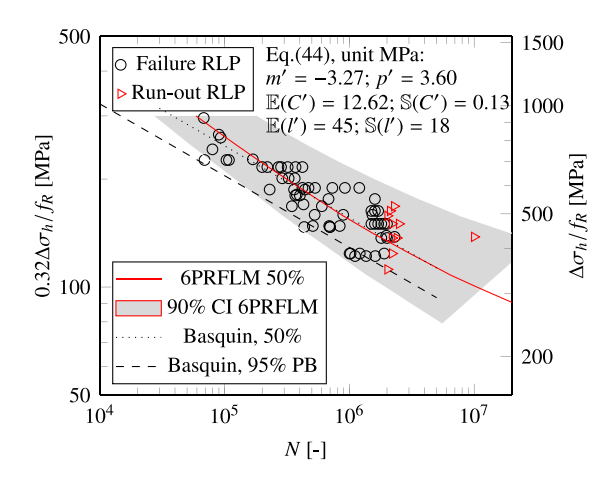


Fig. 16. Fatigue test data of red lead paint (RLP), average and 90% confidence interval (90% CI – 5% and 95% confidence bounds) of the Six Parameter Random Fatigue Limit Model (6PRFLM) and average and 95% prediction bound (PB) of the Basquin equation.

6.2. Proposed fatigue resistance for practice

The data in Fig. 14 show a gradual transition between the finite life and near-infinite life regions. Some models enable to describe this transition, amongst which is the Six Parameter Random Fatigue Limit Model (6PRFLM) [67]:

$$\log_{10}(N) = C' + m' \log_{10}(0.32\Delta\sigma_h) - p' \log_{10}\left(1 - \frac{l'}{0.32\Delta\sigma_h}\right)$$
(44)

We used the maximum likelihood to fit parameters C', m', p' and l' to the test data, in this case including run-outs as right-censored data. Fig. 16 gives the expectation and the 90% confidence interval (CI, having 5% and 95% one-sided confidence bounds) of the model for RLP specimens. The dotted line provides the Basquin equation fitted through the data with an inverse slope m=-5 (ignoring run-outs). This line is in good agreement with the 6PRFLM for the important long-life region $(N>5\cdot 10^5)$ and it is conservative for the less relevant region of shorter life. We therefore base the fatigue resistance for practical use on a Basquin equation with slope m=-5. Note that the number of tests with very-long-life $(N>5\cdot 10^6)$ is limited. The estimation of the slope of the S–N curve can benefit from additional very-long-life tests.

The fatigue resistance is often expressed as the stress range at which the 95% prediction bound coincides with a life of two million cycles. This resistance is $\Delta\sigma_C=111$ MPa / 0.32=349 MPa according to the Basquin equation, with the corresponding S–N curve given as a dashed line in Fig. 16. Using the same slope for specimens with mill scale, the resistance is $\Delta\sigma_C=105$ MPa / 0.32=330 MPa, using the expectations $\mu_{ms}=0.33$ and $\sigma_{cl,0}$ according to Eq. (38) in the model for the hoop stress. The difference between these curves is small. We propose a Basquin curve with slope m=-5 and $\Delta\sigma_C=330$ MPa in the fatigue assessment of riveted double covered joints in existing bridges.

6.3. Stress ratio effect

The stress ratio correction using the net section stress as fatigue driving force is much larger compared to the linear elastic hoop stress, compare Eqs. (2) and (39). Obviously, plasticity takes place at the notch unless the load remains small. Schijve [68] explains that plasticity at the notch significantly influences the local stress ratio for medium load levels, see Fig. 17, whereas the elastoplastic stress range at the notch remains closer to its linear elastic equivalent. Because of this, the correction for stress ratio using linear elastic stress should be smaller for notched components compared to unnotched ones.

Refs. [69–73] give stress ratio corrections or mean stress corrections derived from tests on unnotched specimens of similar steel grades as

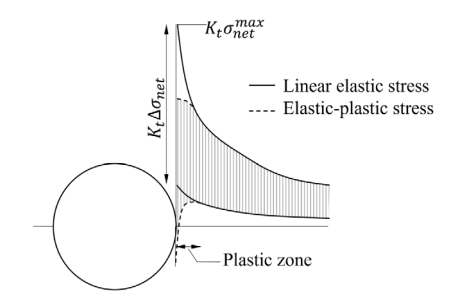


Fig. 17. Effect of plasticity near a notch on the stress range and the stress ratio. Source: Figure based on Schijve [68].

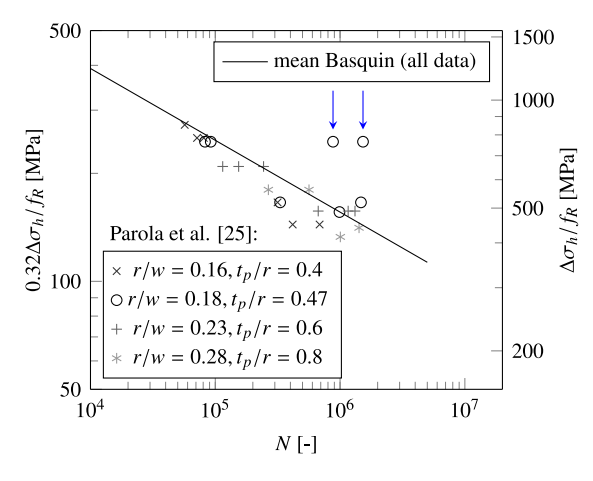


Fig. 18. Fatigue tests of [25] at R = 0, normal clamping. Except for the two marked data, all data are in good agreement with the Basquin curve of the entire database. The two marked data are therefore likely outliers.

used for the hot riveted joints. Compared to these data, the stress ratio correction required for riveted joints using the hoop stress is indeed smaller than that of unnotched specimens. On the contrary, the stress ratio correction required for the net section stress is larger than that of unnotched specimens. This further suggests that the net section stress might not be a good indicator of the fatigue driving force of riveted double covered joints. This is relevant because the only negative stress ratio tested is R = -1. The validity of Eq. (3) for other negative stress ratios is hence unknown.

6.4. Test outliers

Fig. 14(b) shows a few data that significantly deviate from the other data, having a longer or shorter life than the others. To evaluate whether these deviations are due to experimental outliers or caused by a wrong choice of the hoop stress as the fatigue driving force, two of these deviating data - indicated with arrows in Fig. 14(b) - are evaluated hereafter. Fig. 18 provides these data together with the other data of the series to which they belong: source [25], R = 0, specimens with normal clamping. The highlighted tests are part of a series of eleven tests of the same geometry (out of which seven failures), with two of these tested at the same stress range as the highlighted tests. All other data of that series are close to the mean Basquin curve of the full test database. It is therefore likely that the two highlighted tests are experimental outliers. Parola et al. [25] report that the plate surfaces of their specimens were slightly rougher than the mill-scale surfaces in other studies and that the riveting pressure was maintained for a slightly longer time than usual. This may have contributed to the relatively high fatigue resistance of the two tests.

6.5. Relevancy for practice

We will now try to explain the large variation in fatigue resistance based on the net section stress proposed by others. In all cases, the fatigue resistance is defined as the stress range at two million cycles with a 95% survival probability. Taras and Greiner [13] propose a dualslope Basquin equation (m = -3 for high stress ranges and m = -5for low stress ranges) with a fatigue resistance of 80 MPa or 90 MPa, depending on the rivet steel grade, the bearing ratio, and the application of RLP. Their background document [74] shows that their database comprises three sources [20,21,31], almost entirely consisting of joints with $n_{row} = 2$. Despite this uniformity, the fatigue test data plotted in S-N curve format show relatively large scatter. They therefore considered subsets of specimens with mill scale and low bearing ratio, high bearing ratio, and RLP. The proposed fatigue resistance of $\Delta\sigma_C=90$ MPa is a conservative value compared to the 95% survival probability of the first subset, whereas the resistance of $\Delta\sigma_C=80$ MPa follows for the latter two subsets.

Pedrosa et al. [16] propose a fatigue resistance of $\Delta\sigma_C=61$ MPa and an inverse slope of m=-4. Their fatigue resistance is lower than that proposed by the other studies, caused by the large scatter of their collected data. On the contrary, the same author group [15] recommends a relatively high fatigue resistance of 107 MPa and a 'flat' S–N curve with an inverse slope of m=-10. This latter recommendation is based on two tested geometries, namely one with $n_{row}=1$ and one with $n_{row}=2$. The two geometries gave a significantly different fatigue resistance, attributed in [15] to different crack growth properties of the materials involved. Using the analytical model for the hoop stress, however, the difference in geometry forms an additional explanation: the tests with $n_{row}=1$ give a lower fatigue resistance. The large ratio r/w=0.53 of this geometry causes the relatively high fatigue resistance despite of the single rivet row.

Individual test series in [32] result in an extremely high fatigue resistance of up to 227 MPa with an inverse slope of m=-7.7. This value is based on tests with a fortunate geometry, with $n_{row}=2$ and r/w=0.38.

The difference in fatigue resistance of these subsets reduces significantly if based on the hoop stress range. The variation in fatigue resistance between 61 MPa and 227 MPa (factor 3.7) proposed by these references based on the net section stress reduces to between 94/0.32 MPa and 110/0.32 MPa (factor 1.2) based on the hoop stress and a slope parameter m = -5. (This comparison excludes one series in [15] because of lacking data on the specimen geometry.)

The predicted fatigue resistance using the hoop stress range differs significantly from that based on the net section stress range. Note that the test database does not cover the full range of geometries applied in joints in bridges. As an example, consider a long joint with one or two rivets in Row 1 and an increasing number of rivets in subsequent rows. Such a joint may have a ratio r/w < 0.15 and $n_{row} > 4$, the values being the extreme bounds of the test data. Assessment of such joints requires a sound, mechanics-based evaluation method. The net section stress range is not fulfilling this requirement. For these reasons, we advice against evaluating the fatigue resistance of riveted double covered joints with the net section stress range and we advocate the use of the hoop stress range instead.

7. Conclusions

This study evaluates the fatigue driving force of hot riveted double covered joints failing in the ply. Considered candidates for the fatigue driving force are the net section stress and the hoop stress in the plate. Whereas others have employed the FE method to estimate the hoop stress range, this study provides an analytical model for the estimation. Such a model enables efficient evaluation of the hoop stress range for a wide range of geometries and load cases. It also gives insight into

how the joint geometry influences the fatigue resistance. We applied the model to a large database of fatigue test results.

The main finding is that the net section stress range is an inaccurate predictor of the fatigue resistance. Using a Basquin equation with an inverse slope of m=-5, the standard deviation of the 10-th base logarithm of the number of cycles to failure is large: $\mathbb{S}(C)=0.44$. The fatigue resistance evaluated with the net section stress range heavily depends on the joint geometry. The hoop stress range is a much more accurate predictor of the fatigue resistance. The fatigue resistance is then largely independent of geometry and the standard deviation is $\mathbb{S}_C=0.34$ or 0.25 for the subsets with mill scale contact and with RLP, respectively. A quantitative probabilistic analysis reveals that the aleatory uncertainties in friction coefficient and clamping force cause the difference between these two subsets.

Based on these findings, the net section stress should be used with great caution in the assessment of riveted double covered joints. This is especially important for larger joints, which often have dimensions outside the range of test data.

Using the analytical model for the hoop stress, with friction coefficients of 0.33 for mill scale contact or 0.06 for red lead paint, and Eq. (38) for the clamping stress, we recommend a Basquin equation for practical assessments with an inverse slope m=-5 and a (linear elastic) hoop stress range of $\Delta\sigma_h=330$ MPa at 2 million cycles, which provides the 95% lower prediction bound.

CRediT authorship contribution statement

Johan Maljaars: Writing – original draft, Validation, Methodology, Formal analysis, Conceptualization. **Sjoerd Hengeveld:** Writing – review & editing, Methodology, Formal analysis. **Jorrit Rodenburg:** Writing – review & editing, Formal analysis.

Declaration of competing interest

The authors declare that they have no known competing financial interests or personal relationships that could have appeared to influence the work reported in this paper.

Acknowledgement

We thank Rijkswaterstaat for sponsoring this study.

Appendix A. Supplementary data

Supplementary material related to this article can be found online at https://doi.org/10.1016/j.ijfatigue.2024.108466.

References

- [1] Collette Q. Riveted connections in historical metal structures (1840-1940). hot-driven rivets: Technology, design and experiments (Ph.D. thesis), Vrije Universiteit Brussel; 2014.
- [2] Righiniotis TD, Imam BM, Chryssanthopoulos MK. Fatigue analysis of riveted railway bridge connections using the theory of critical distances. Eng Struct 2008;30(10):2707–15.
- [3] Pipinato A, Pellegrino C, Bursi OS, Modena C. High-cycle fatigue behavior of riveted connections for railway metal bridges. J Constr Steel Res 2009;65:2167–75.
- [4] Pipinato A, Molinari M, Pellegrino C, Bursi OS, Modena C. Fatigue tests on riveted steel elements taken from a railway bridge. Struct Infrastruct Eng 2011;7(12):907–20.
- [5] Marques F, Correia JA, de Jesus AM, Cunha A, Caetano E, Fernandes AA. Fatigue analysis of a railway bridge based on fracture mechanics and local modelling of riveted connections. Eng Fail Anal 2018;94:121–44.
- [6] Bertolesi E, Buitrago M, Adam JM, Calderón PA. Fatigue assessment of steel riveted railway bridges: Full-scale tests and analytical approach. J Constr Steel Res 2021;182:106664.
- [7] Horas CS, Silva JN, Correia JA, De Jesus AM. Fatigue damage assessment on aging riveted metallic railway bridges: A literature review. Structures 2023;58:105664.

- [8] Fisher JW, Yen BT, Wang D. Fatigue strength of riveted bridge members. J Struct Eng 1990:116(11):2968–81.
- [9] Brühwiler E, Smith IF, Hirt MA. Fatigue and fracture of riveted bridge members. J Struct Eng 1990;116(1):198–214.
- [10] DiBattista JD, Adamson DE, Kulak GL. Fatigue strength of riveted connections. J Struct Eng 1998;124(7):792-7.
- [11] COWI. Guideline for load and resistance assessment of existing European railway bridges. Tech. rep., COWI; 2007.
- [12] Kühn B, Lukic M, Nussbaumer A, et al. Assessment of existing steel structures: recommendations for estimation of remaining fatigue life. Tech. rep., Joint Research Center: 2008.
- [13] Taras A, Greiner R. Development and application of a fatigue class catalogue for riveted bridge components. Struct Eng Int 2010;20(1):91–103.
- [14] Sanches RF, De Jesus AM, Correia JA, Da Silva A, Fernandes A. A probabilistic fatigue approach for riveted joints using Monte Carlo simulation. J Constr Steel Res 2015;110:149–62.
- [15] Pedrosa B, Correia JA, Rebelo C, Lesiuk G, De Jesus AM, Fernandes AA, et al. Fatigue resistance curves for single and double shear riveted joints from old Portuguese metallic bridges. Eng Fail Anal 2019;96:255–73.
- [16] Pedrosa B, Correia JA, Rebelo CA, Veljkovic M. Reliability of fatigue strength curves for riveted connections using normal and Weibull distribution functions. ASCE-ASME J Risk Uncertain Eng Syst A 2020;6(3):04020034.
- [17] Sanchez L, Gutierrez-Solana F, Pesquera D. Fatigue behaviour of punched structural plates. Eng Fail Anal 2004;11:751–64.
- [18] Wilson WM, Thomas FP. Fatigue tests of riveted joints. University of Illinois; 1938.
- [19] Graf O. Dauerversuche mit Nietverbindungen in St37 zur Erkennung des Einflusses von σ : τ . Bauingenieur 1932;29/30:389–93.
- [20] Graf O. Versuche im stahlbau dauerversuche mit nietverbindungen. Berichte Deutschen Ausschusses Stahlbau 1935;5:1–61
- [21] Graf O. Versuche mit Nietverbindungen Berichte des Deutschen Ausschusses für Stahlbau Heft 12. Springer-Verlag; 1941.
- [22] Baron F, Larson EW. The effect of grip on the fatigue strength of riveted and bolted joints. In: Proc. 52th ann. conv. AREA. 1953, p. 175–90.
- [23] Baron F, Larson EW. Comparison of bolted and riveted joints. In: Proc. separate no. 470, centenniel convocation III. 1954, p. 1322–34.
- [24] Baron F, Larson EW, Kenworthy KJ. The effect of certain rivet patterns on the fatigue and static strengths of joints. Tech. rep., Northwestern University; 1955.
- [25] Parola JF, Chesson E, Munse W. Effect of bearing pressure on fatigue strength of riveted connections. University of Illinois; 1965.
- [26] Lewitt C, Chesson E, Munse WH. The effect of rivet bearing on the fatigue strength of riveted joints. Tech. rep., University of Illinois; 1959.
- [27] Imam BM, Righiniotis TD, Chryssanthopoulos MK. Numerical modelling of riveted railway bridge connections for fatigue evaluation. Eng Struct 2007;29(11):3071–81.
- [28] Correia JA, da Silva AL, Xin H, Lesiuk G, Zhu S-P, de Jesus AM, et al. Fatigue performance prediction of S235 base steel plates in the riveted connections. Structures 2021;30:745–55.
- [29] De Jesus AM, da Silva AL, Correia JA. Fatigue of riveted and bolted joints made of puddle iron – An experimental approach. J Constr Steel Res 2015;104:81–90.
- [30] Gallegos Mayorga L, Sire S, Correia JA, De Jesus AM, Rebelo C, Fernández-Canteli A, et al. Statistical evaluation of fatigue strength of double shear riveted connections and crack growth rates of materials from old bridges. Eng Fract Mech 2017;185:241–57.
- [31] Klöppel K. Gemeinschaftversuche zur bestimmung der schwellzugfestigkeit voller, gelochter und genieteter Stäbe aus St37 und St52. Bautechnik 1936;13/14:96–112.
- [32] Silva A, Correia J, Xin H, Lesiuk G, De Jesus A, Augusto Fernandes A, et al. Fatigue strength assessment of riveted details in railway metallic bridges. Eng Fail Anal 2021;121:105120.
- [33] Jia D, Zhang Q, Xiong L, Li J, Bu Y, Bao Y. A unified evaluation method for fatigue resistance of riveted joints based on structural stress approach. Int J Fatigue 2022;160:106871.
- [34] Maljaars J, Leonetti D, Maas C. Fatigue life prediction of hot riveted double covered butt joints. Int J Fatigue 2019;124:99–112.
- [35] Wilson WM. Flexural fatigue strength of steel beams, bulletin 45. University of Illinois: 1948.
- [36] Steinhardt O, Valtinat G. Versuche an nietloch-schweissverbindungen. Bauingenieur 1965;363–8.
- [37] Steinhardt O, Möhler K, Valtinat G. Versuche zur anwendung vorgespannter schrauben im stahlbau – IV. teil. Berichte Deutschen Ausschusses Stahlbau 1969:25:106–11
- [38] Hansen NG. Fatigue tests of high-strength steel. Trans ASCE 1961;126:750-63.
- [39] Lenzen K. The effect of various fasteners on the fatigue strength of a structural joint. AREA Bull 1949;480:17–27.

- [40] UIC. Statistische Auswertung von Ermüdungsversuchen an Nietverbindungen in Flussstahl. Office de Recherches et d'Essais, Union Internationale des Chemins de fer (ORE UIC): 1986.
- [41] Livieri P, Lazzarin P, Mutignani F, Tisalvi M. Fatigue tests on riveted connections. In: Proc. 9th nordic steel constr. conf., 2001, p. 599–606.
- [42] DB. Richtlinie RL 805 Tragsicherheit Bestehender Eisenbahnbrücken. Tech. rep., Deutsche Bahn; 2002.
- [43] Imam B, Chryssanthopoulos M, Frangopol D. System effects on the fatigue reliability of deteriorating riveted railway bridges. In: Safety, reliability and risk of structures, infrastructures and engineering systems: proc. 10th int. conf. structural safety and reliability. 2009, p. 1–8.
- [44] De Jesus AMP, Silva AL, Correia JAFO. Fatigue of riveted and bolted joints made of puddle iron — A numerical approach. J Constr Steel Res 2014;102:164–77.
- [45] Horas C, De Jesus A, Rui C. Efficient computational approach for fatigue assessment of riveted connections. J Constr Steel Res 2019;153:1–18.
- [46] Leonetti D, Maljaars J, Snijder H. Fatigue life prediction of hot-riveted shear connections using system reliability. Eng Struct 2019;186:471–83.
- [47] Liu Z, Correia J, Carvalho H, Mourão A, De Jesus A, Calçada R, et al. Global-local fatigue assessment of an ancient riveted metallic bridge based on submodelling of the critical detail. Fatigue Fract Eng Mater Struct 2019;42(2):546–60.
- [48] N677:1993. Klinknagels met bolle kop. Centraal Normalisatie Bureau; 1933.
- [49] Kulak GL, Fisher JW, Struik JHA. Guide to design criteria for bolted and riveted joints. second ed.. American Institute of Steel Construction (AISC; 2001.
- [50] Maljaars J, Euler M. Fatigue S-N curves of bolts and bolted connections for application in civil engineering structures. Int J Fatigue 2021;151:106355.
- [51] Tate M, Rosenfeld S. Preliminary investigation of the loads carried by individual bolts in bolted joints – Technical note no. 1051. Tech. rep., Nasa; 1946.
- [52] Nelson W, Bunin B, Hart-Smith. Critical joints in large composite aircraft structure – contract report 3710. Tech. rep., Nasa; 1946.
- [53] McCarthy M, McCarthy C, Padhi G. A simple method for determining the effects of bolt-hole clearance on load distribution in single-column multi-bolt composite joints. Compos Struct 2006;73(1):78–87.
- [54] Konkong N, Phuvoravan K. An analytical method for determining the load distribution of single-column multibolt connection. Adv Civ Eng 2017;2017:1912724.
- [55] Hutchinson J. Shear coefficients for timoshenko beam theory. J Appl Mech 2000;68(1):87–92.
- [56] 2230:2015 V. Systematic calculation of high duty bolted joints. VDI; 2015.
- [57] Heywood RB. Designing by photoelasticity. Chapman and Hall; 1952.
- [58] Yang Z, Kim CB, Cho C, Beom HG. The concentration of stress and strain in finite thickness elastic plate containing a circular hole. Int J Solids Struct 2008;45:713–31.
- [59] Valtinat G. Neue Entwicklungen im konstruktiven Ingenieurbau. Tech. rep., Technical University Karlsruhe; 1994.
- [60] Zhou Y. Fatigue strength evaluation of riveted bridge members (Ph.D. thesis), Lehigh University: 1994.
- [61] Åkesson B, Edlund B. Fatigue life of riveted railway bridges (Ph.D. thesis), Chalmers University; 1994.
- [62] Leonetti D, Maljaars J, Pasquarelli G, Brando G. Rivet clamping force of as-built hot-riveted connections in steel bridges. J Constr Steel Res 2020;167:105955.
- [63] Riedel T, Sieber L, Flederer H. Influence of rivet clamping stress on fatigue crack growth behaviour. ce/papers 2021;4(2-4):1145-52.
- [64] Taylor D. The theory of critical distances. Eng Fract Mech 2008;75(7):1696-705.
- [65] Livieri P. Numerical analysis of double riveted lap joints. Lubricants 2023;11(9):396.
- [66] Bartsch H, Feldmann M. Revision of fatigue detail categories of plain members and mechanically fastened joints according to EC3-1-9. J Constr Steel Res 2021;179:106549.
- [67] Leonetti D, Maljaars J, Snijder HH. Fitting fatigue test data with a novel S-N curve using frequentist and Bayesian inference. Int J Fatigue 2017;105:128–43.
- [68] Schijve J. Introduction to fatigue of structures and materials. Springer; 2001.
- [69] Smith JO. The effect of range of stress on the fatigue strength of metals; Bulletin no. 334. Tech. rep., University of Illinois; 1942.
- [70] Frost NE, Marsh KJ, Pook LP. Metal fatigue. Clarendon Press; 1974.
- [71] Morrow J. Fatigue design handbook. SAE Pub. No. AE-4; 1968.
- [72] Dowling N, Calhoun C, Arcari A. Mean stress effects in stress-life fatigue and the walker equation. Fatigue Fract Eng Mater Struct 2009;32(3):163–79.
- [73] Morgantini M, MacKenzie D, Comlekci T, van Rijswick R. The effect of mean stress on corrosion fatigue life. Procedia Eng 2018;213:581–8.
- [74] Taras A, Greiner R. Statische Festigkeit und Ermüdungsfestigkeit genieteter Bauteile - Auswertung der Versuchsdaten und Bemessungsvorschläge. Tech. rep., Graz University of Technology; 2007.